Impact of an Exponential Profile of Saturated Hydraulic Conductivity within the ISBA LSM: Simulations over the Rhône Basin

B. DECHARME, H. DOUVILLE, A. BOONE, F. HABETS, AND J. NOILHAN

Météo-France/CNRM, Toulouse, France

(Manuscript received 29 September 2004, in final form 27 May 2005)

ABSTRACT

This study focuses on the influence of an exponential profile of saturated hydraulic conductivity, k_{sat}, with soil depth on the water budget simulated by the Interaction Soil Biosphere Atmosphere (ISBA) land surface model over the French Rhône River basin. With this exponential profile, the saturated hydraulic conductivity at the surface increases by approximately a factor of 10, and its mean value increases in the root zone and decreases in the deeper region of the soil in comparison with the values given by Clapp and Hornberger. This new version of ISBA is compared to the original version in offline simulations using the Rhône-Aggregation high-resolution database. Low-resolution simulations, where all atmospheric data and surface parameters have been aggregated, are also performed to test the impact of the modified k_{sat} profile at the typical scale of a climate model. The simulated discharges are compared to observations from a dense network consisting of 88 gauging stations.

Results of the high-resolution experiments show that the exponential profile of k_{sat} globally improves the simulated discharges and that the assumption of an increase in saturated hydraulic conductivity from the soil surface to a depth close to the rooting depth in comparison with values given by Clapp and Hornberger is reasonable. Results of the scaling experiments indicate that this parameterization is also suitable for large-scale hydrological applications. Nevertheless, low-resolution simulations with both model versions overestimate evapotranspiration (especially from the plant transpiration and the wet fraction of the canopy) to the detriment of total runoff, which emphasizes the need for implementing subgrid distribution of precipitation and land surface properties in large-scale hydrological applications.

1. Introduction

Land surface models (LSMs) were introduced in atmospheric general circulation models (AGCMs) to provide realistic lower boundary conditions to temperature and moisture. The complexity of these models ranges from the simple bucket model (Manabe 1969) to more sophisticated soil–vegetation–atmosphere transfer (SVAT) schemes with multiple parameterizations representing the physical processes linked to vegetation, soil, and snow. Although these models have been significantly improved over recent decades, hydrologic applications still remain a challenge for state-of-the-art LSMs. A new approach that consists of coupling LSMs with river routing schemes appears to be a powerful tool for understanding the regional and global water cycles (Dümenil and Todini 1992; Habets et al. 1999b; Oki et al. 1999), predicting streamflow (Habets et al. 2004), and thus improving SVAT parameterizations (Lohmann et al. 1998; Chapelon et al. 2002; Boone et al. 2004).

LSMs are used on a wide range of spatial scales, including at very low resolutions when they are coupled to AGCMs. Therefore, the influence of scaling on the LSM parameterizations, especially for hydrological applications, appears as a critical problem (Wood et al. 1998; Lohmann et al. 1998; Dirmeyer et al. 1999). Along these lines, the Rhône-Aggregation (Rhône-AGG) LSM intercomparison project was recently undertaken at Météo-France (Boone et al. 2004). The first goal of Rhône-AGG was to investigate how different LSMs simulate the river water balance at high resolution for several annual cycles compared to observed data from a dense network of gauging stations. It was shown that the subgrid runoff formulation is particularly important for simulating realistic daily discharges over the Rhône River basin. The second goal of the

Corresponding author address: Bertrand Decharme, Météo-France, CNRM/GMGEC/UDC, 42 ave. G. Coriolis, 31057 Toulouse, France.
E-mail: bertrand.decharme@cnrm.meteo.fr

project was to examine the impact of changing the horizontal resolution on the simulations. Results from a series of scaling experiments were examined in which the spatial resolution was decreased to be more consistent with that of AGCMs. The general conclusion was that LSMs that take account of land surface and/or atmospheric forcing spatial heterogeneities are able to reduce the scaling influence on the simulated water budget.

In addition to surface heterogeneities, other physical soil processes exert a significant influence on river discharge and soil moisture. For example, many studies revealed that the organic matter and the living and decayed root systems have a strong impact on soil hydraulic conductivity. Water movement into the soil is generally favored in the uppermost few centimeters (Delire et al. 1997). Roots create relatively large continuous openings, which serve as conducting channels for rapid movement of water in forest soil profiles (Gaiser 1952). Over a local watershed forested area, Harr (1977) pointed out that soil structural characteristics affect hydrologic properties more than textural properties. Texture and total porosity changed little with depth but saturated hydraulic conductivity, k_{sat}, decreased significantly, and pore-size distribution changed markedly. After and during a storm event, both the magnitude and the direction of the water flux in the soil and the subsoil varied temporally. Moreover, the maximum fluxes in the top meter were greater than those in the subsoil. These observations are consistent with the assumption of surface macropores that favor water movement in the soil surface (Beven 1982a). Beven (1982b) proposed that the decrease of k_{sat} and porosity could be estimated using exponential relationships. He showed, from a wide range of in situ data, that there was no significant relationship between both exponential profiles and that the decrease of k_{sat} was much more rapid than that of porosity, which could be neglected (Beven 1984). Vertically homogeneous soil porosity is therefore a reasonable assumption when assuming an exponential profile of k_{sat}. Coupling these works with a statistical approach that takes into account the spatial variability of the catchment topography, Beven and Kirkby (1979) and Sivapalan at al. (1987) proposed a simple hydrological forecasting model, named TOPMODEL, that takes account of the strong influence of topography on the generation of soil moisture heterogeneity and runoff. Famiglietti and Wood (1994) were the first to introduce both the exponential profile of k_{sat} and the TOPMODEL formalism in an LSM at a catchment scale. This work, like that of Sivapalan et al. (1987), accounts for saturation excess runoff generation (Dunne process) via TOPMODEL, but also includes a separate infiltration excess mechanism (Horton runoff) using a Philip approximation to the infiltration capacity. Based on these studies, Stieglitz et al. (1997) performed a comparison between a single-column model where k_{sat} was taken to be vertically homogeneous, and another single-column model where k_{sat} declined with depth and was much higher by a factor 100 in the first soil centimeters. Then, they showed that the exponential profile had an influence on simulated river discharge. The introduction of this decrease of k_{sat} in an LSM revealed that the so-called compacted values of k_{sat} (Chen and Kumar 2001) used by climate modelers, given for example by Brooks and Corey (1966) or Clapp and Hornberger (1978), could be much lower than those used by hydrologists in the soil surface layers (Beven 1982b). Then, with the same approach as Stieglitz et al. (1997), Chen and Kumar (2001) proposed that k_{sat} reaches its so-called "compacted" value at a depth of 1 m and increases by approximately a factor 10 at the surface. However, one can question whether an increase of k_{sat} in the first soil meter, below which it reaches its hypothetical compacted value, is a realistic assumption. This formalism was applied at the local scale (Niu and Yang 2003), as well as at the continental scale (Chen and Kumar 2001) with a model resolution more consistent with that of AGCMs. Nevertheless, one can also wonder what is the impact of an exponential profile of k_{sat} on the simulated water budget sensitivity to spatial aggregation.

Using the Rhône-AGG dataset, the first goal of the present study is to examine the relevance of the approach of Chen and Kumar (2001) to simulate the land surface water budget at a regional scale. The second objective is to examine the influence of the exponential profile of k_{sat} on the simulated water budget sensitivity to spatial aggregation in order to investigate if this approach is also suitable for global hydrological applications. A simple parameterization of the k_{sat} profile is introduced in the Interaction Soil Biosphere Atmosphere (ISBA) scheme, which only depends on two parameters: the rate of decline of the k_{sat} profile and the depth where k_{sat} reaches its compacted value. The hydraulic conductivity profile can be generalized by a power function (Ambroise et al. 1996; Duan and Miller 1997; Iorgulescu and Musy 1997). Nevertheless, this kind of function depends on an additional shape parameter that would be difficult to calibrate at the global scale. So the simpler formalism of Chen and Kumar (2001) is here chosen. An overview of the original ISBA LSM and details of the exponential profile parameterization are presented in section 2. The Rhône-AGG modeling system is briefly reviewed in section 3. The results of the experiments are shown in section 4.

A sensitivity study to the new parameters is presented in section 5. A final discussion and the conclusions are provided in sections 6 and 7, respectively.

2. The ISBA land surface model

a. Overview of the model

The initial ISBA LSM was developed at Météo-France by Noilhan and Planton (1989) and implemented in the Météo-France atmospheric GCM by Manzi and Planton (1994) and Mahfouf et al. (1995) and more recently in the Canadian Regional Weather Forecast Model by Bélair et al. (2003). ISBA contains the basic physics of the land surface. The model is relatively simple and needs only a limited number of parameters, which depend on the type of soil and vegetation. It uses the force–restore method (Deardorff 1977, 1978) to calculate the time evolution of the surface and mean soil temperature. The water budget is based on a soil hydrology, a rainfall interception scheme (Noilhan and Mahfouf 1996), and a one-layer snow scheme (Douville et al. 1995). Note that a more complex snow scheme is also available (Boone and Etchevers 2001) but is not used in the present study as the more simple snow scheme is currently used in the climate model. The model also simulates freezing and thawing in the two uppermost layers (Boone et al. 2000).

The original ISBA LSM had only a two-layer soil hydrology: a thin surface layer with a uniform depth, d_1 (m), included in the total soil layer. More recently, a third layer was introduced by Boone et al. (1999) in order to distinguish between the rooting depth, d_2 (m), and the total soil depth, d_3 (m). In other words, the ISBA LSM now has a three-layer soil hydrology: the root zone layer overlaps the surface layer, whereas the deep-soil reservoir extends from the base of the root zone to the base of the modeled soil column. The governing equations for the time (t) evolution of soil moisture for each layer are written as follows:

$$\frac{\partial w_1}{\partial t} = \frac{C_1}{\rho_w d_1}(I_r - E_{\text{soil}}) - D_1 - \frac{F_{1w}}{\rho_w d_1}, \tag{1}$$

$$\frac{\partial w_2}{\partial t} = \frac{1}{\rho_w d_2}(I_r - E_{\text{soil}} - E_{\text{transp}}) - K_2 - D_2 - \frac{F_{2w}}{\rho_w d_2}, \tag{2}$$

$$\frac{\partial w_3}{\partial t} = \frac{d_2}{(d_3 - d_2)}(K_2 + D_2) - K_3, \tag{3}$$

where w_1, w_2, and w_3 represent the layer-average volumetric water contents ($m^3\ m^{-3}$) for the surface, root zone, and deep soil layers, respectively. The volumetric water content within each reservoir is constrained to be less than the soil porosity or saturation water content, w_{sat} ($m^3\ m^{-3}$); ρ_w ($kg\ m^{-3}$) is the density of liquid water and C_1 is the dimensionless surface force–restore soil transfer coefficient for moisture (Braud et al. 1993; Giordani et al. 1996). In Eqs. (1) and (2), E_{soil} and E_{transp} ($m\ s^{-1}$) represent bare soil evaporation and plant transpiration respectively. Plant transpiration stops when w_2 is below the wilting point volumetric water content, w_{wilt} ($m^3\ m^{-3}$), corresponding to a matric potential of –150 m; F_{1w} and F_{2w} are the surface and subsoil net phase change, which represent mass fluxes ($kg\ m^{-2}\ s^{-1}$) from either soil ice production or melt (Boone et al. 2000); and D (s^{-1}) is the vertical soil moisture diffusion, which is proportional to the C_2 and C_4 dimensionless diffusion restore coefficients (Noilhan and Planton 1989; Boone et al. 1999).

The variable I ($m\ s^{-1}$) represents the infiltration rate given by the difference between the throughfall rate, P_g ($m\ s^{-1}$), and the surface runoff, Q_s ($m\ s^{-1}$). The throughfall rate is the sum of three components: the rainfall not intercepted by the canopy, the dripping from the interception reservoir, and the snowmelt from the snowpack. The surface runoff, which only takes into account the Dunne mechanism, is calculated through the use of a new TOPMODEL formalism. This surface runoff formulation was validated over the French Ardèche river basin by Habets and Saulnier (2001) using the two-layer soil hydrology version. In this study, the coupling between ISBA and TOPMODEL is generalized to the three-layer version (appendix A). The main difference is that the spatial distribution of the topographic index in each grid cell is computed with the three-parameter gamma distribution introduced by Sivapalan et al. (1987) (appendix B).

The variable K (s^{-1}) represents gravitational drainage, which is proportional to the C_3 drainage restore coefficient (Mahfouf and Noilhan 1996); K was modified in order to enable a linear residual drainage when the soil moisture of each layer is below the field capacity, w_{fc} ($m^3\ m^{-3}$). The idea is to take account of spatial heterogeneity of soil moisture and soil hydraulic properties within a grid box (Habets et al. 1999b; Etchevers et al. 2001). This residual drainage is not specifically calibrated for the Rhône basin but was tuned in global hydrological simulations. When the k_{sat} exponential profile option is used, no drainage occurs below the wilting point. The assumption is that water is globally linked with the root and pore into the soil when this one is dry. In addition, if the soil moisture of the third layer exceeds the soil porosity, a saturation excess subsurface runoff is generated. Note that the drainage or subsurface runoff, Q_{sb}, generated by ISBA is the sum of the deep-drainage, K_3, and of the saturation excess run-

off of each layer. The subsurface runoff formalism given by TOPMODEL is not used here (see appendix A). (A schematic representation of ISBA is shown later in Fig. 2.)

Finally, all force–restore terms (C_1, C_2, C_3, and C_4) and soil hydrological parameters (w_{sat}, w_{wilt}, and w_{fc}) are related to soil textural properties and moisture using the parameter expressions and values from Clapp and Hornberger (1978), Noilhan and Mahfouf (1996), and Boone et al. (1999). These expressions relate hydraulic conductivity, k (m s^{-1}), and matric potential, ψ (m), to each volumetric soil water content w_i at level i as a function of soil type (Brooks and Corey 1966; Clapp and Hornberger 1978):

$$\psi(w_i) = \psi_{sat}\left(\frac{w_i}{w_{sat}}\right)^{-b} \quad (i = 1, 3), \tag{4a}$$

$$k(w_i) = k_{sat,c}\left(\frac{w_i}{w_{sat}}\right)^{-2b+3} \quad (i = 1, 3), \tag{4b}$$

where $k_{sat,c}$ (m s^{-1}) is the compacted value of the saturated hydraulic conductivity given by Clapp and Hornberger (1978), ψ_{sat} (m) is the saturated soil water potential or air entry potential, and b is the dimensionless slope of the soil moisture retention curve.

b. Exponential profile of k_{sat}

Montaldo and Albertson (2001) have already studied the impact of an exponential profile of soil hydraulic properties in the ISBA LSM, but in the case of stratified soils. They introduced a textural layering effect, representing this exponential profile, in the two-layer version of ISBA. They showed that this exponential profile improved the soil moisture content of both layers in comparison with observed data. In this study, this approach is generalized to the three-layer soil hydrology, but with vertically homogeneous soil textures in absence of detailed field information on soil stratification.

As already mentioned in the introduction, the chosen formalism is close to the one proposed by Chen and Kumar (2001):

$$k_{sat}(z) = k_{sat,c} \times e^{-f(z-d_c)}, \tag{5a}$$

$$k(w_i, z) = k_{sat}(z)\left(\frac{w_i}{w_{sat}}\right)^{-2b+3}, \tag{5b}$$

where z (m) is the depth of the soil profile and f (m^{-1}) is the exponential profile decay factor. This formalism assumes that at the compacted depth, d_c (m), k_{sat} reaches the compacted value, $k_{sat,c}$, given by Clapp and Hornberger (1978). The hydraulic conductivity profile in the original version of ISBA is assumed to be vertically homogeneous [Eq. (4b)]. Thus, the parameterization of an exponential profile of k_{sat} involves a simple recalculation of all force–restore coefficients introduced in section 3a and now named C_1', C_2', C_3', and C_4'.

The surface restore coefficient, C_1, is directly proportional to the root square of the inverse of the first layer's saturated hydraulic conductivity (Noilhan and Planton 1989). For estimating C_1', the original coefficient C_1 is multiplied by a quantity representing the average saturated hydraulic conductivity, $\overline{k}_{sat,1}$, in the first layer. Because the first layer is very thin (0.01 m), its average saturated hydraulic conductivity value is close to the saturated hydraulic conductivity at the surface($z = 0$): $\overline{k}_{sat,1} \approx k_{sat}(0)$. Then, to substitute Eq. (5a) into the surface restore coefficient, C_1, leads to

$$C_1' = C_1 \times \sqrt{\frac{1}{e^{fd_c}}}. \tag{6}$$

The coefficient C_2 characterizes the velocity at which the water profile is restored to its equilibrium. It increases or decreases with hydraulic conductivity. Noilhan and Planton (1989) proposed that the C_2 coefficient depends on soil moisture and is proportional to C_{2ref}, which is a function of soil texture. Thus, for taking account of the influence of the k_{sat} profile in layers one and two, the value of C_{2ref} is empirically adjusted. Hence, according to Noilhan and Planton (1989), the C_2' coefficient is given by

$$C_2' = \left(C_{2ref} + \tau\frac{\overline{k}_{sat,2} - k_{sat,c}}{d_2}\right) \times \left(\frac{w_2}{w_{sat} - w_2}\right) = C_2 + \tau\frac{\overline{k}_{sat,2} - k_{sat,c}}{d_2}\left(\frac{w_2}{w_{sat} - w_2}\right), \tag{7a}$$

$$\overline{k}_{sat,2} = \frac{1}{d_2}\int_0^{d_2} k_{sat}(z)\,dz = k_{sat,c}\frac{[e^{fd_c} - e^{f(d_c - d_2)}]}{fd_2}, \tag{7b}$$

where τ (s) is a time constant of one day, and $\overline{k}_{sat,2}$ is the saturated hydraulic conductivity averaged over the root zone profile. In Eq. (1), the diffusion term, D_1, in the right-hand side represents the diffusion of water in the soil. It depends on a restoring term, which characterizes the effect of the vertical gradient of hydraulic potential (Noilhan and Planton 1989). However, Montaldo and Albertson (2001) showed that the structure of this restoring term is not directly adaptable to a soil model with an exponential profile of hydraulic properties. The value of the surface volumetric water content at the balance of gravity and capillary forces, w_{geq} (m^3 m^{-3}), is

a function of w_2 and of soil textures with adjustments to account for the relative importance of capillarity and gravity forces (Noilhan and Planton 1989). Hence, if w_1 is greater than this equilibrium value, w_{geq}, then the surface layer is expected to be draining to the root zone, and if w_1 is less than w_{geq}, the upper layer is expected to be recharging from below. However, Montaldo and Albertson (2001) have shown that ISBA could erroneously predict a significant upward flow in the surface layer for a soil with an exponential profile. Thus, they proposed to adjust the w_2 value for the calculation of the C_2 coefficient and w_{geq} term. Similarly, the new parameterization presented in this paper assumes that when the surface and root layers are in equilibrium ($w_2 = w_1$), both equalities $\psi(w_1) = \psi(w_2)$ and $k(w_1) = k(w_2)$ must be satisfied because ISBA assumes vertically homogeneous soil textural properties. This is the case for the first equation [Eq. (4a)], but not for the second as it is shown by Eq. (5). Therefore, with the same idea as in Montaldo and Albertson (2001) and after combining several algebraic steps starting from Eq. (5b), the w_2 value for the C_2 and w_{geq} calculation is adjusted as follows:

$$w_2' = w_2 \left[\frac{\overline{k}_{\text{sat},2}}{k_{\text{sat}}(0)} \right]^{(1/2b+3)}. \tag{8}$$

The C_3 coefficient characterizes the rate at which the water profile is restored to the field capacity for a soil layer with a thickness of 1 m. Its analytical expression, which can be found in Mahfouf and Noilhan (1996), is directly proportional to the average saturated hydraulic conductivity of each layer. Then, both C_3' coefficients (for layers two and three, respectively) are estimated as follows:

$$C_{3,2}' = C_3 \frac{\overline{k}_{\text{sat},2}}{k_{\text{sat},c}} = C_3 \frac{[e^{fd_c} - e^{f(d_c - d_2)}]}{fd_2}, \tag{9a}$$

$$C_{3,3}' = C_3 \frac{\overline{k}_{\text{sat},3}}{k_{\text{sat},c}} = C_3 \frac{[e^{f(d_c - d_2)} - e^{f(d_c - d_3)}]}{f(d_3 - d_2)}, \tag{9b}$$

where $\overline{k}_{\text{sat},3}$ is the average saturated hydraulic conductivity over the deep layer profile.

Finally, the diffusion restore coefficient C_4, which was calibrated by taking into account the grid geometry of both subsurface soil layers, is also directly proportional to the average saturated hydraulic conductivity between the midinterval of layers two and three (Boone et al. 1999). In this case, the C_4' coefficient was parameterized as follows:

$$C_4' = \frac{C_4}{k_{\text{sat},c}} \times \frac{2}{d_3} \int_{(d_2/2)}^{(d_3 + d_2/2)} k_{\text{sat}}(z)\, dz$$

$$= C_4 \frac{2}{fd_3} [e^{f(d_c - (d_2/2))} - e^{f(d_c - (d_3 + d_2/2))}]. \tag{10}$$

Note that this new parameterization was tested against in situ observations with the experimental dataset used by Mahfouf and Noilhan (1991) and with the Monitoring the Useable Soil Reservoir Experimentally (MUREX) field experiment dataset (Calvet et al. 1999). Comparisons with observed soil moisture and energy fluxes showed satisfactory results (not shown). Moreover, simulations with the multilayer version of ISBA (with explicit resolution of the diffusion equations; Boone et al. 2000) confirm that the exponential profile of k_{sat} has a positive impact especially on the simulated soil water profile.

3. Experiment design

a. Brief overview of the GEWEX Rhône project

The Rhône is the largest European river flowing into the Mediterranean Sea. The Rhône basin covers over 95 000 km^2 mostly in southeastern France (Fig. 1). Soil and vegetation characteristics, subsurface parameters, and atmospheric forcing are mapped onto this domain under the auspices of the Global Energy and Water Cycle Experiment (GEWEX) Rhône project (http://www.cnrm.meteo.fr/mc2/projects/rhoneagg/), which was conceived in recent years by the French research community in order to study the continental water cycle on the regional scale. The Rhône aggregation dataset is described in detail in Boone et al. (2004).

The domain is divided up into 1471 8 km × 8 km grid boxes. The atmospheric forcing is calculated using the Analysis System for Providing Atmospheric Information Relevant to Snow (SAFRAN) analysis system (Durand et al. 1993). The input atmospheric data consist of standard screen-level observations at approximately 60 Météo-France weather network sites within the domain. The data are recessed over 249 homogeneous climatic zones, and total daily precipitation data from over 1500 gauges. All of the common forcing variables are available at a 3-h time interval. Four years of forcing are used in the current study, starting 1 August 1985 and ending 31 July 1989. The 4-yr monthly mean rainfall and snowfall rates are shown in Fig. 1. Solid precipitation is mainly concentrated over the alpine region. For liquid precipitation, orographic effects play an important role, with the strongest rates observed near the Cévennes, Jura, and Vosges mountains. Total pre-

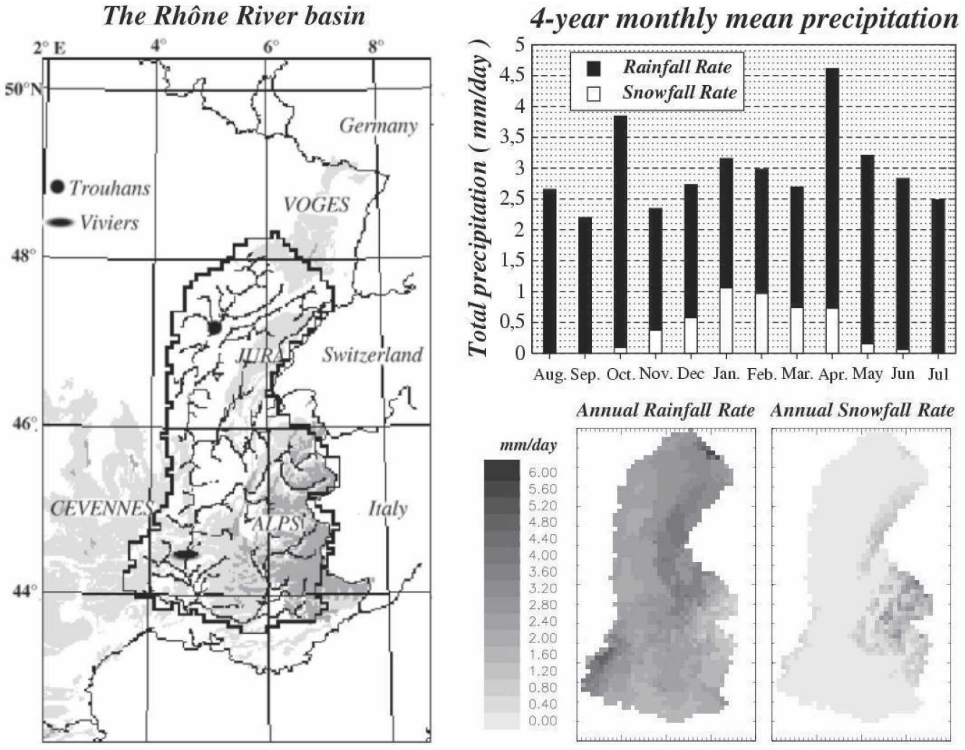

FIG. 1. Representation of the (left) Rhône River basin, (right top) monthly mean basin-average precipitation rate, and (right bottom) spatial distribution of the annual mean rainfall and snowfall rates. Mountainous areas (in gray) and the Trouhans (plain circle) and Viviers (plain oval circle) gauging stations are shown.

cipitation has a weak interannual variability even if the third year is slightly wetter than the others [see Etchevers et al. (2001) for further details on the atmospheric forcing].

Soil and vegetation data are available at the same spatial resolution as the atmospheric forcing. Soil parameters are defined using the soil textural properties from the National Institute of Agronomical Research (INRA) soil database (King et al. 1995). Vegetation parameters are defined using a vegetation map from the Corine Land Cover Archive (Giordano 1992) and a 2-yr satellite archive of the Advanced Very High Resolution Radiometer/normalized difference vegetation index (AVHRR/NDVI; Champeaux et al. 2000).

In addition to both the SAFRAN analysis system and the ISBA LSM, another component of the Rhône-AGG modeling system is the MODCOU distributed hydrological model (Habets et al. 1999a). MODCOU is used to convert the surface runoff and the drainage produced by ISBA into river discharge and water table variations (Fig. 2). The surface runoff is transferred to the river, and the routing from each grid cell is based on isochronous zones using a time step of one day. The drainage acts as a source for the water table, which is modeled using the diffusivity equations. The version of the MODCOU model used in the present study is slightly different from this used in the Rhône-AGG project. The routing in the river and the relation between the aquifer and the river is computed over the reach for all river gauges and not only for the one connected to the aquifer.

It is important to note that the three components of the modeling system were developed and validated independently. Further details related to the offline experiment design can be found in Habets et al. (1999b).

b. Experiments

The ISBA LSM is integrated with a 5-min time step for four consecutive annual cycles, but the first year is treated as a spinup year. Results are validated over the last three years (August 1986 to July 1989). Three kinds of experiments are performed. The first two are aimed at validating ISBA with (ISBA-exp) and without (ISBA) the exponential profile of k_{sat}. The third one is a sensitivity study to the k_{sat} exponential profile parameters, d_c and f.

For the first two experiments, the control simulation consists of running ISBA over the high-resolution grid

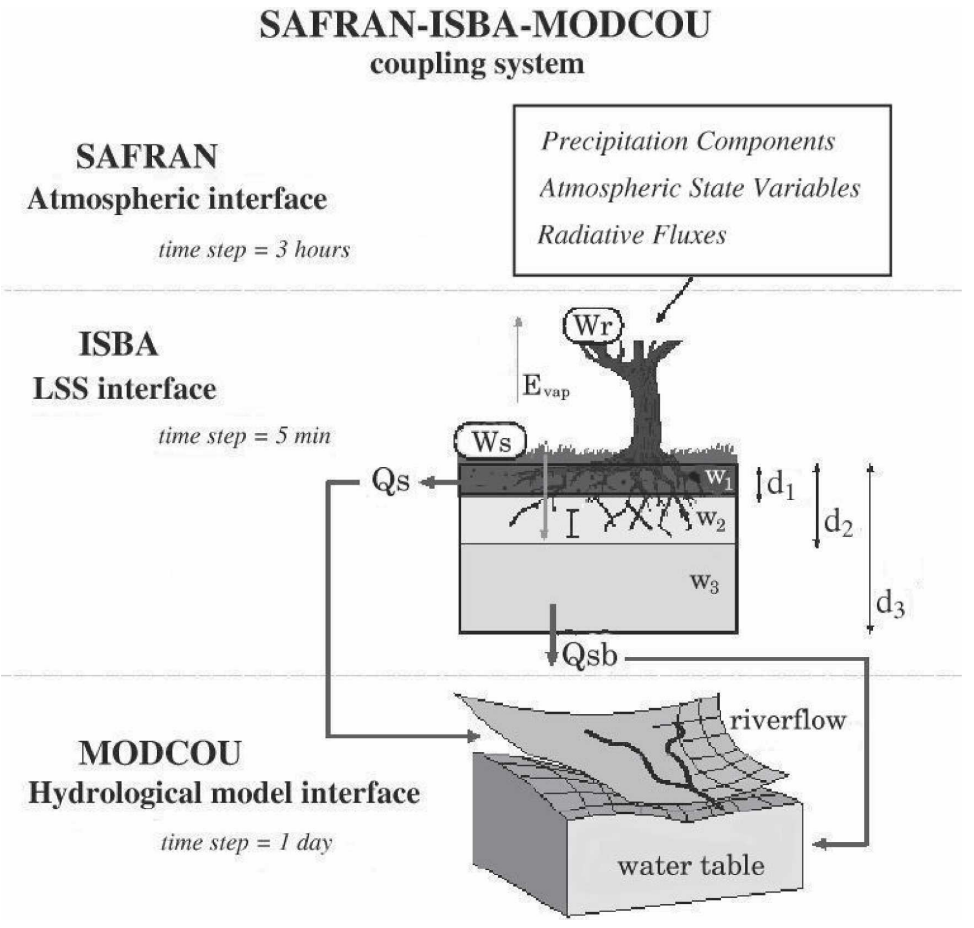

FIG. 2. Schematic representation of the SAFRAN–ISBA–MODCOU coupling system. All variables are defined in section 3a.

(8 km × 8 km). The range and average of each land surface parameter over the entire domain are shown in Table 1. The simulated total runoff is used to drive the MODCOU hydrological model, and the simulated discharges are compared to observed data. The set of observations that is used for evaluating the ISBA simulations over the Rhône basin consists of daily streamflow data from 88 river gauges. Only subbasins where damming does not impact the flow too much are used for the validation (Etchevers et al. 2001; Habets et al. 1999b). The second experiment is based on the same protocol. The only difference is that simulations are performed at a low resolution (1° × 1°) after aggregating all atmospheric data and surface parameters (more details can be found in Boone et al. 2004). Because the MODCOU model is integrated over the high-resolution grid, the simulated runoff is linearly disaggregated to the 8 km by 8 km grid before it is transferred to the hydrological model. The purpose of this experiment is to address two issues:

- First, how does the upscaling affect the simulated water budget components?
- Second, is the exponential profile of k_{sat} also suitable for global hydrological applications?

Finally, for the sensitivity study to the d_c and f parameters, the various values for each parameter are summarized in Table 2. These simulations are performed only on the high-resolution grid in order to explore briefly how these two parameters affect the simulated water budget components and river discharges, and to give some general perspectives. Note that one simulation is performed with the hypothesis of Beven (1997) who proposed a proportional relationship between the f and M parameters if a constant "drained porosity" is assumed in the model. Here, M (m) is a coefficient that describes the exponential decrease of the soil transmissivity with local deficit into the TOPMODEL formalism (see appendix A). In ISBA, like in most LSMs, soil textural properties are

TABLE 1. Land surface parameter values averaged over the Rhône River basin (entire 8 km by 8 km resolution domain). Hydrological parameters from Noilhan and Lacarrère (1995) are also shown. The average in both space and time is provided for parameters with the "—monthly" denotation.

Variable description	Symbol	Avg	Range	Units
Superficial soil depth	d_1	0.01	—	m
Rooting depth	d_2	1.54	(2.00, 1.00)	m
Total soil depth	d_3	2.25	(3.00, 1.00)	m
Clay fraction	X_{clay}	0.22	(0.47, 0.04)	—
Sand fraction	X_{sand}	0.31	(0.89, 0.07)	—
Soil porosity	w_{sat}	0.46	(0.49, 0.40)	$\text{m}^3\ \text{m}^{-3}$
Field capacity volumetric water content	w_{fc}	0.23	(0.34, 0.15)	$\text{m}^3\ \text{m}^{-3}$
Wilting point volumetric water content	w_{wilt}	0.17	(0.26, 0.07)	$\text{m}^3\ \text{m}^{-3}$
Hydraulic conductivity at saturation	$k_{\text{sat, }c}$	6.75	(181, 1.31)	$\times 10^{-6}\ \text{m s}^{-1}$
Matric potential at saturation	ψ_{sat}	−0.39	(−0.61, −0.11)	m
b parameter	b	6.43	(9.94, 4.05)	—
Snow-free surface albedo	α	0.17	(0.20, 0.15)	—
Minimum stomatal resistance	$R_{s\,\min}$	74.91	(150, 40.0)	s m^{-1}
Leaf area index—monthly	LAI	1.93	(4.00, 0.00)	$\text{m}^2\ \text{m}^{-2}$
Snow-free surface roughness—monthly	z_0	0.29	(1.00, 0.01)	m
Vegetation cover fraction—monthly	veg	0.58	(0.91, 0.00)	—

homogeneous over the entire soil column. Then, the drained porosity can be related to the difference between the saturation and lower-level water contents that permits drainage. ISBA with the exponential profile of k_{sat} assumes no drainage below wilting point (cf. section 2), and thus the relationship between the f and M parameters can be written as

$$f = \frac{w_{\text{sat}} - w_{\text{wilt}}}{M}. \tag{11}$$

4. Results

In the validation experiments, the soil column in the ISBA-exp simulation assumes an exponential profile of k_{sat} where the compacted depth, d_c, is defined as the rooting depth with the assumption that roots and organic matter favor the development of macrospore and facilitate the water movements. Furthermore, below the rooting depth, the soil compaction effect implies more difficult water movements in the deep soil. In local-scale applications, f is generally calibrated, but, at a regional or a global scale, it is not possible and a constant value of 2 m^{-1} is here used over the entire Rhône River basin. In other words, k_{sat} at the surface increases by approximately a factor of 10, and its mean value grows in the root zone and decreases in the deeper region of the soil in comparison with a vertically homogeneous profile of k_{sat} (see Table 2). These values provide optimal river discharge simulations, as the sensitivity analysis will show in section 6.

a. High-resolution experiments

1) SURFACE HYDROLOGICAL FLUXES

The comparison in Fig. 3 shows that the partitioning of total annual mean precipitation between total runoff ($Q_s + Q_{\text{sb}}$) and evapotranspiration (E_{vap}) in the ISBA-

TABLE 2. Summary of the sensitivity study experiments. The control run is similar to the ISBA-exp simulation in section 4. The basin-average $k_{\text{sat}}(0)/k_{\text{sat},c}$ and $\overline{k}_{\text{sat},i}/k_{\text{sat},c}$ ratios of each layer (i = 2, 3) are shown (denoted Avg) as well as the corresponding ranges over the entire domain.

	$k_{\text{sat}}(0)/k_{\text{sat},c}$		$\overline{k}_{\text{sat},2}/k_{\text{sat},c}$		$\overline{k}_{\text{sat},3}/k_{\text{sat},c}$	
Simulations	Avg	Range	Avg	Range	Avg	Range
d_c = 0.0 m (f = 2 m^{-1})	1.00	—	0.32	(0.42, 0.25)	0.03	(0.13, 0.01)
d_c = 1.0 m (f = 2 m^{-1})	7.34	—	2.33	(3.19, 1.81)	0.23	(1.00, 0.06)
d_c = 1.5 m (f = 2 m^{-1})	20.10	—	6.33	(8.68, 4.93)	0.63	(2.71, 0.16)
Control run (ISBA-exp)	25.60	(54.60, 7.40)	7.44	(13.40, 3.19)	0.54	(1.00, 0.43)
f = 1 m^{-1} ($d_c = d_2$)	4.88	(7.39, 2.72)	2.43	(3.19, 1.72)	0.72	(1.00, 0.63)
$f \sim M^{-1}$ ($d_c = d_2$)	54.60	—	13.40	—	0.47	(2.99, 0.43)
f = 3 m^{-1} ($d_c = d_2$)	144.00	(403.00, 20.10)	27.70	(67.10, 6.36)	0.42	(0.99, 0.32)

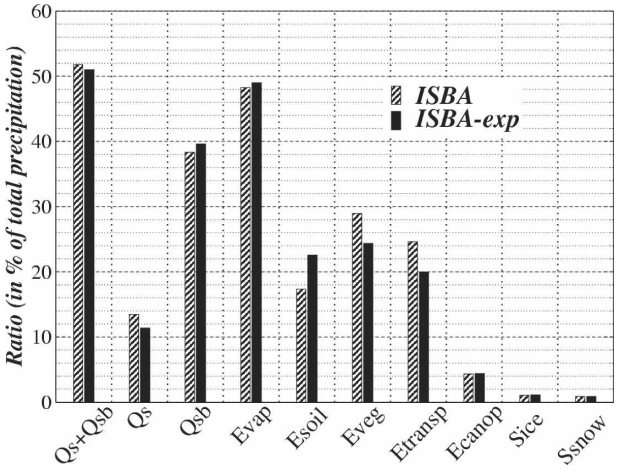

FIG. 3. Comparison of the Rhône basin water budget simulated by ISBA (dashed bar) and ISBA-exp (plain bars) at the high resolution. The annual mean basin-average ratios of total runoff (Q_s+Q_{sb}), surface runoff (Q_s), drainage (Q_{sb}), evapotranspiration (E_{vap}), bare soil evaporation (E_{soil}), vegetation evapotranspiration (E_{veg}), plant transpiration (E_{transp}), canopy interception loss (E_{canop}), ice sublimation (S_{ice}), and snow sublimation (S_{snow}) to total precipitation are expressed in %. Note that $E_{veg} = E_{transp} + E_{canop}$.

exp simulation is slightly more balanced (51%/49%) than in the ISBA simulation, which tends to favor total runoff at the expense of E_{vap} (52%/48%). The partitioning between surface runoff (Q_s) and drainage (Q_{sb}) is more contrasted. With the exponential profile, the drainage is clearly reduced. The $Q_s/(Q_s + Q_{sb})$ (surface runoff/total runoff) ratio decreases from 0.26 for ISBA to 0.22 for ISBA-exp. Nevertheless, the main difference between both model versions is that the exponential profile clearly induces an increase in bare soil evaporation (E_{soil}) to the detriment of the plant transpiration (E_{transp}). Note that ice sublimation (S_{ice}) and snow sublimation (S_{snow}) are quite small over the entire Rhône basin.

2) SOIL MOISTURE

Soil moisture is a key hydrological variable because it controls the partitioning of precipitation between runoff and evapotranspiration. For quantifying the soil water content, a normalized index named soil wetness index (SWI) can be defined as follows:

$$\mathrm{SWI} = \frac{w_{\mathrm{tot}} - w_{\mathrm{wilt}}}{w_{\mathrm{fc}} - w_{\mathrm{wilt}}}, \tag{12}$$

where w_{tot} represents the total volumetric soil water content ($m^3\ m^{-3}$) since the ISBA top layer (w_1) is included in the rooting reservoir (w_2). The SWI takes a value of 0 when the soil water content is at the wilting point and a value of 1 at the field capacity.

For the whole period, ISBA-exp shows a general deficit in soil moisture in comparison with ISBA (Fig. 4). On the one hand, the lower states of SWI equilibrium and of moisture equilibrium in the root layer (w_2) are directly related because the water storage capacity of the rooting reservoir is larger than that of the deep reservoir. On the other hand, the volumetric water content of the deep reservoir (w_3) in ISBA-exp is larger than in ISBA. These results are consistent with an increase of k_{sat} from the rooting depth to the surface (related to ISBA), which favors upward water fluxes to the surface and downward water fluxes to the deep reservoir. The increase in upward water diffusion favors bare soil evaporation to the detriment of plant transpiration. Furthermore, the decrease of k_{sat} in the deep soil favors water storage and thus drainage. Accordingly, ISBA-exp shows a drier rooting layer that involves a weaker surface runoff than in ISBA because

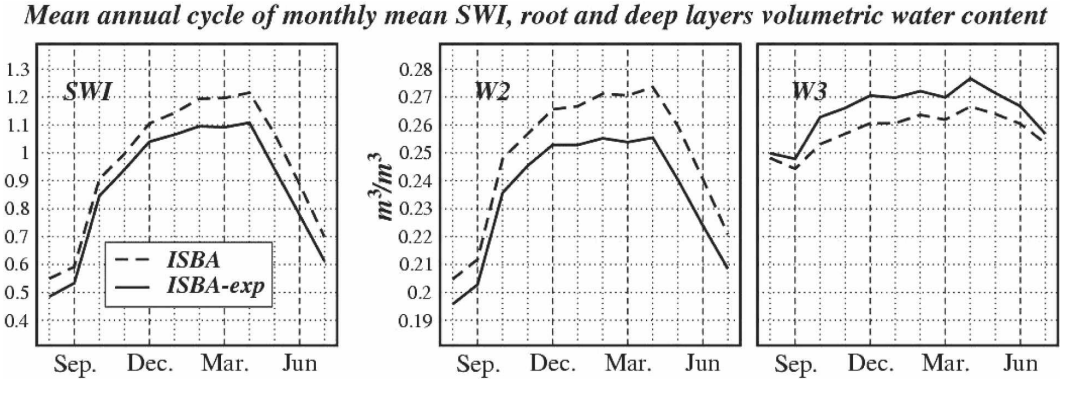

FIG. 4. Mean annual cycle of the monthly mean SWI, and root and deep layer volumetric water contents, denoted w_2 and w_3 respectively.

surface runoff is directly related to the root layer water content (see appendixes A and B).

3) DISCHARGES

The simulated discharges are validated at Trouhans and Viviers, which are located in the northern and southern parts of the basin (Fig. 1), in Figs. 5a and 5b, respectively. Observed data from Trouhans are used to evaluate the discharge simulations over a small basin ($\sim$900 km^2). The mouth of the Rhône River is not used here for the validation over the entire basin because dams greatly influence this station. Nevertheless, a more reasonable model evaluation over a large portion of the basin (81%) can be done using observed data from Viviers. The statistics are shown in Table 3 where Eff represents efficiency or Nash–Sutcliffe criterion (Nash and Sutcliffe 1970), and $Q_{\text{sim}}/Q_{\text{obs}}$ represents the annual simulated/observed discharge ratio. Here Eff measures the skill of the model at capturing the observed variability of the discharges. It is defined as follows:

$$\text{Eff} = 1.0 - \frac{\sum_{t=1,N} [Q_{\text{sim}}(t) - Q_{\text{obs}}(t)]^2}{\sum_{t=1,N} [Q_{\text{sim}}(t) - \overline{Q_{\text{obs}}}]^2}, \qquad (13)$$

where $\overline{Q_{\text{obs}}}$ represented the observed temporal mean; Eff can be negative if the simulated discharge is very poor, is above 0.5 for a reasonable simulation, above 0.7 for a good one, and would be 1 for a perfect model (Boone et al. 2004).

For the two models at each station $Q_{\text{sim}}/Q_{\text{obs}}$ is close to 1, indicating that both model versions simulate the annual discharge well over the entire period. The monthly Eff also shows good results, but it is difficult to decide which model version is the best at this time scale. The daily Eff leads to the same conclusion even if ISBA-exp shows a positive impact on the quality of the simulated discharges at Trouhans. This advantage is mainly due to an improved discharge dynamics as shown in Fig. 6 where composites from about 10 rainy events (crosses in Fig. 5) are shown for both stations. Even if both model versions show a lack of discharge production during the rainy events, ISBA-exp shows a better behavior, especially after the peak of runoff.

A global discharge validation based on a daily efficiency comparison (Fig. 7) is also performed with the help of 88 gauging stations distributed over the entire basin. The number of stations, where the efficiency is high, is larger for ISBA-exp than for ISBA. For example, the efficiencies of ISBA-exp and ISBA are greater than 0.7 at 22% and 11% of the gauging station respectively. Furthermore, the mean value of Eff grows from 0.52 for ISBA to 0.55 for ISBA-exp (Table 4). The station-by-station comparison [number of stations with best Eff (NSBE) in Table 4] reveals that there are 69 gauging stations for a total of 88 where the ISBA-exp efficiencies are improved compared to ISBA.

b. Low-resolution experiments

1) WATER BUDGET SENSITIVITY

In both model versions, the upscaling effect induces an increase in evapotranspiration and a decrease in total runoff (Fig. 8a) in keeping with conclusions of Rhône-AGG (Boone et al. 2004). The overestimation of the evapotranspiration at the low resolution is mainly due to the plant transpiration and the canopy interception loss (E_{canop}). The increase in interception loss at the low resolution is a well-known response to the aggregated precipitation. The spatial average involved by upscaling reduces the precipitation rates and increases the spatial coverage of a rainfall event (Dolman and Blyth 1997; Boone et al. 2004; Vérant et al. 2004). The total runoff deficit is clearly due to surface runoff and drainage discrepancies, especially during the summer, and early autumn. The poor root-mean-square error (rmse) (Fig. 8b) between monthly total runoff simulated at the high and low resolutions mainly results from this drastic underestimation during this period. The main reason is the forcing aggregation, and not just the aggregation of precipitation, that leads to warmer and dryer conditions at low resolution (Boone et al. 2004), and thus favors evapotranspiration. In addition, the ice and snow sublimation are underestimated at a low resolution (Fig. 8a) because these warmer conditions involve a deficit in simulated snow mass and soil ice content (Boone et al. 2004). Finally, the upscaling of vegetation and soil properties also tends to favor plant transpiration instead of total runoff (not shown).

ISBA-exp shows a relatively weaker sensitivity to spatial aggregation for total runoff and evapotranspiration (Fig. 8). Surface runoff sensitivity is clearly re-

→

FIG. 5. Time series of the observed (black points) and simulated (blue line for ISBA and red line for ISBA-exp) monthly mean and daily river discharges at (a) Trouhans and (b) Viviers. The location of these gauging stations is shown in Fig. 1. Black crosses show the selected storm events for the composite analysis provided in Fig. 6.

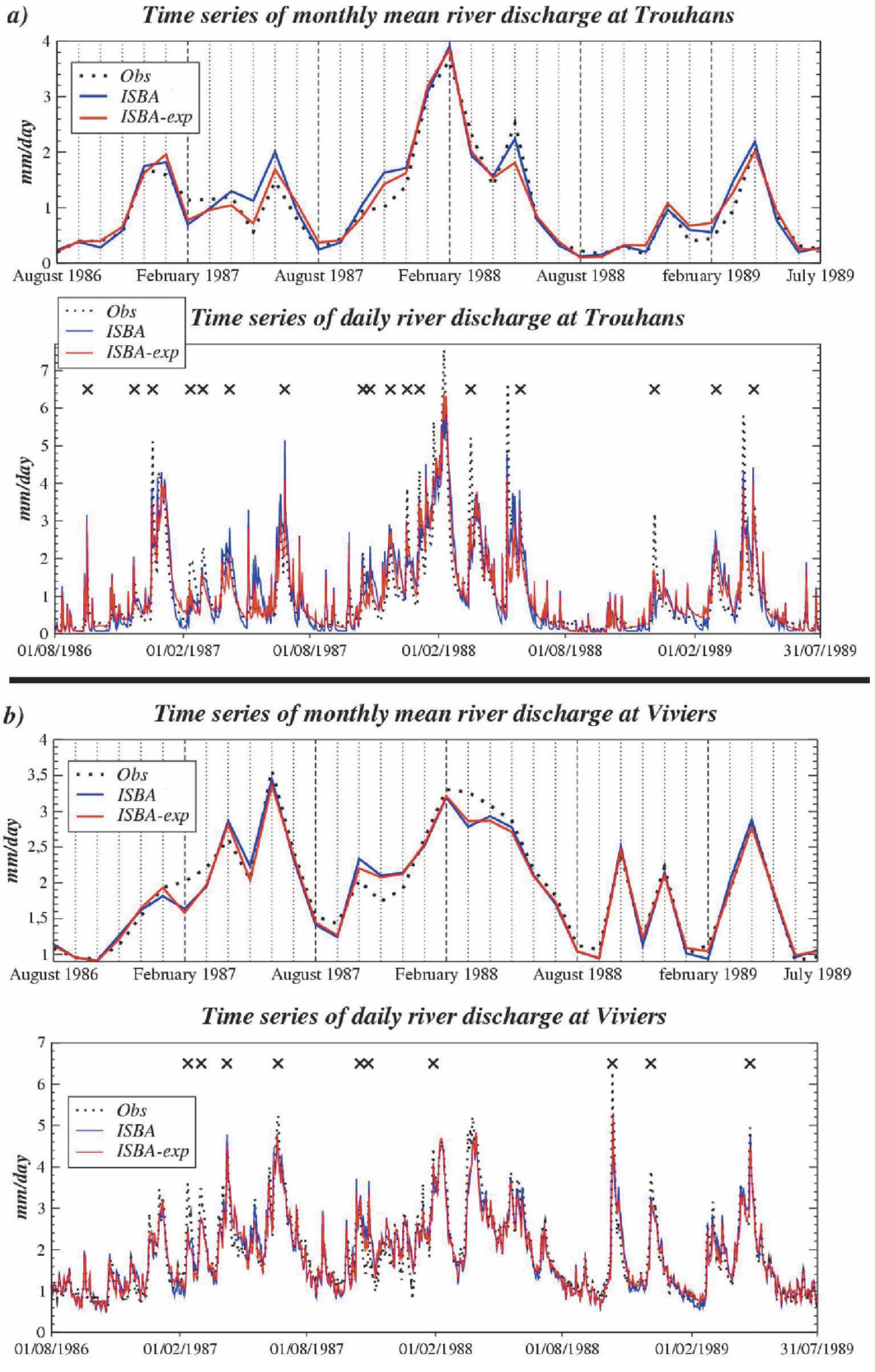
a)
Time series of monthly mean river discharge at Trouhans
Obs
ISBA
ISBA-exp
mm/day
August 1986
February 1987
August 1987
February 1988
August 1988
february 1989
July 1989
Time series of daily river discharge at Trouhans
01/08/1986
01/02/1987
01/08/1987
01/02/1988
01/08/1988
01/02/1989
31/07/1989
b)
Time series of monthly mean river discharge at Viviers
Time series of daily river discharge at Viviers

TABLE 3. Statistics of simulated monthly and daily river discharges at Trouhans and Viviers. Definitions of Q_{sim}/Q_{obs} and efficiency (Eff) are given in section 4a(3).

Gauging stations	Simulations	Q_{sim}/Q_{obs}	Eff	
			Monthly	Daily
Trouhans	ISBA	1.06	0.91	0.75
	ISBA-exp	1.04	0.93	0.81
Viviers	ISBA	0.99	0.94	0.89
	ISBA-exp	0.98	0.95	0.91

duced but it is not the case for drainage. The exponential profile tends also to reduce the sensitivity of plant transpiration and bare soil evaporation. In other words, the exponential profile of k_{sat} shows a positive impact on the water budget sensitivity to model resolution.

2) DISCHARGES

The same validation as in section 4a(3) is performed. The cumulative daily efficiency distribution of ISBA-exp (Fig. 9) shows improved results. Furthermore, the comparison station by station shows that the ISBA-exp efficiencies are improved at 73 of the 88 gauging stations (Table 5). The mean value grows from 0.39 for ISBA to 0.42 for ISBA-exp.

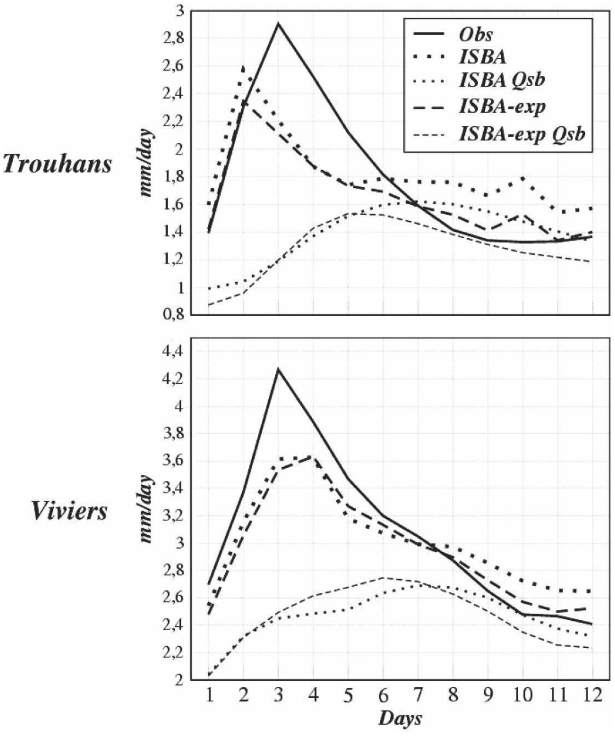

FIG. 6. Discharge composites of storm event at (top) Trouhans and (bottom) Viviers. The selected storm events are shown in Fig. 5. For both stations, the composite time series start 2 days before the observed storm and finish 9 days afterward. Observations, ISBA, and ISBA-exp are represented in solid, dotted, and dashed lines, respectively. For both simulations, the routed drainage (Q_{sb}) is also shown.

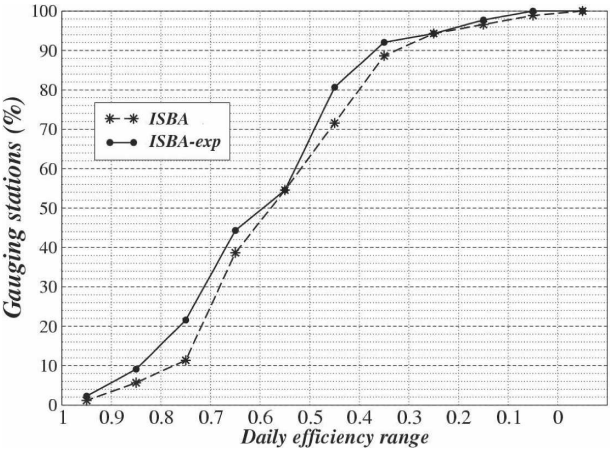

FIG. 7. Cumulative efficiency distributions of daily river discharges simulated at high resolution. The dashed and solid lines represent the ISBA and ISBA-exp distributions, respectively. These distributions are computed from a dense observational network consisting of daily discharges at 88 gauging stations. Statistics about these distributions are given in Table 4.

5. Sensitivity tests

The two last experiments consist of running ISBA-exp at the high resolution with the different values of the compacted depth and f (Table 2). In the first experiment, the compacted depth varies from a value of 0 to 1.5 m (f fixed to 2 m^{-1}) in order to investigate the impact on the simulated water budget over the Rhône basin of variation in k_{sat} in the first meter of the soil relative to the values given by Clapp and Hornberger (1978). The second experiment consists of running ISBA-exp with f varying from a value of 1 to 3 m^{-1} (the compacted depth fixed to the rooting depth). The simulation with f proportional to the M parameter of TOPMODEL [Eq. (11)] is named the M simulation.

TABLE 4. Statistics of the efficiency distribution of the simulated daily river discharges at the high resolution. The minimum (min), mean (mean), maximum (max), and standard deviation (std dev) of the distribution are shown. The number of stations with the best Eff (NSBE) is also represented.

Eff distribution statistics	ISBA	ISBA-exp
Min	−0.01	0.05
Mean	0.52	0.55
Max	0.90	0.91
Std dev	0.19	0.19
NSBE	19	69

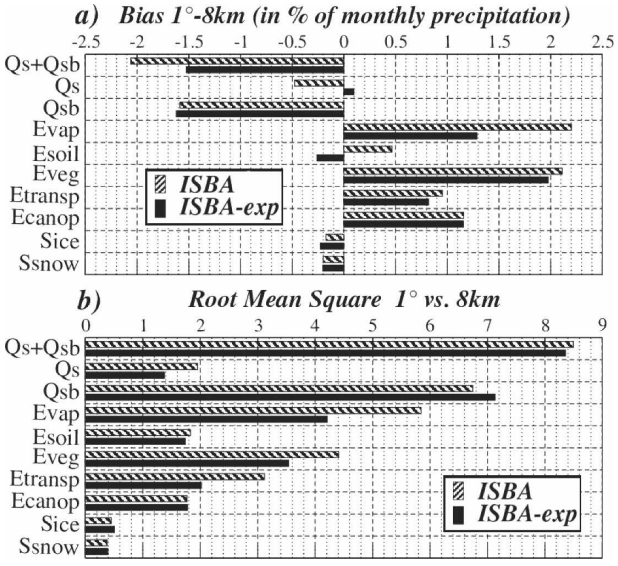

FIG. 8. Impact of scaling on the simulated water budget. The low-resolution experiment (1° × 1°) is compared to the high-resolution experiment (8 km × 8 km). The (a) bias and (b) root-mean-square error of surface hydrological fluxes are calculated using the basin-average ratio of each monthly mean flux ($\overline{\text{Flux}}_{\text{month}}$) to monthly mean precipitation ($\overline{\text{P}}_{\text{month}}$) in %: $100 \times (\overline{\text{Flux}}_{\text{month}}/\overline{\text{P}}_{\text{month}})$ (month = 1, 2, 3 . . . , 36). Notations are the same as in Fig. 3.

For this simulation, f has a basin-average value of 2.68 m^{-1} with a range of 2 to 4 m^{-1}. In these two experiments, the control run is the ISBA-exp simulation with the same configuration as in section 5 (the compacted depth fixed to the rooting depth and $f = 2\ \text{m}^{-1}$).

a. Surface hydrological fluxes

The compacted depth has a weak influence on the partitioning of precipitation into total runoff and evapotranspiration (Fig. 10a), but f alters notably this partitioning (Fig. 10b). Nevertheless, the partitioning of total runoff into surface runoff and drainage, as well as the partitioning of evapotranspiration into bare soil evaporation and plant transpiration, is slightly more sensitive to the compacted depth than to f. The increase of f favors clearly surface runoff instead of drainage, as well as plant transpiration. This is also true, though less marked, for the compacted depth. More generally, the increase of both f and the compacted depth leads to an increase in runoff at the expense of evapotranspiration.

These results are not surprising. When the compacted depth and/or f increase, the hydraulic conductivity is increased in the root layer. The augmentation of upward flows from this layer to the surface leads to an increase in bare soil evaporation and the downward flow to the deep soil is also favored. Then, the root layer water content decreases, so that surface runoff decreases, as well as plant transpiration. Moreover, when the compacted depth increases, k_{sat} is also increased in the deep layer, and drainage is favored. Nevertheless, when f increases, k_{sat} decreases in the deep layer. Thus, the deep layer water content increases, and, finally, drainage is favored. Note that the saturation excess subsurface runoff is not negligible when the compacted depth equals 0 and 1 m (respectively 37.7% and 2% of drainage). It occurs because the strong decrease in k_{sat} in the deep layer leads to the saturation of the lowest reservoir.

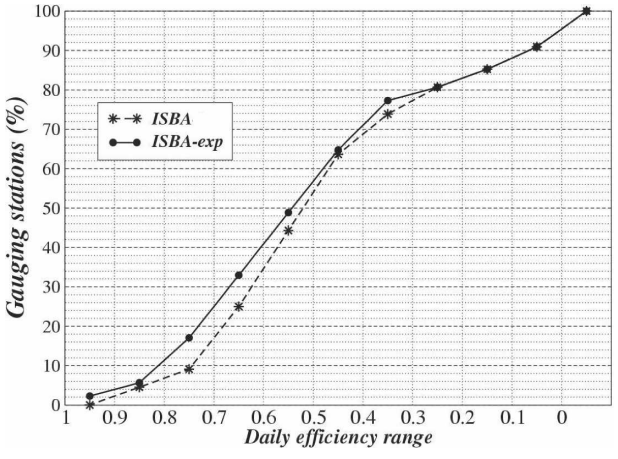

FIG. 9. Cumulative efficiency distributions of daily river discharges simulated at low resolution. Notations are the same as in Fig. 7. Statistics about these distributions are given in Table 5.

TABLE 5. As in Table 4, but for statistics of the efficiency distribution of the simulated daily river discharges at the low resolution.

Eff distribution statistics	ISBA	ISBA-exp
Min	−1.50	−1.75
Mean	0.39	0.42
Max	0.90	0.91
Std dev	0.35	0.39
NSBE	15	73

b. Discharges

Apart from the control run, the simulation obtained with a compacted depth of 1.5 m (Fig. 11a) and the M simulation (Fig. 11b) show the best results. The mean values of Eff (0.55 and 0.54, respectively) are close to those obtained in the control run (Table 6). Furthermore, the simulation with a compacted depth of 1.5 m has the best daily efficiencies at 45 gauging stations against 37 for the simulation without compacted depth ($d_c = 0$ m) and only 6 for a compacted depth of 1 m. The M simulation has the best daily efficiencies at 50

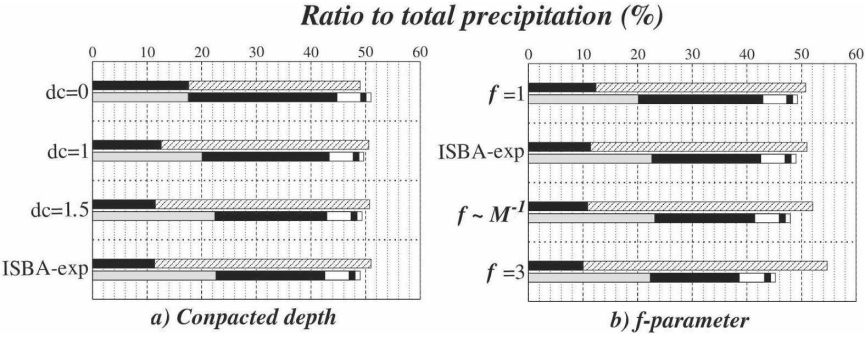

FIG. 10. Sensitivity to (a) the compacted depth, d_c, and to (b) the f parameter of the water budget simulated at high resolution. Values of d_c and f are given in Table 2. The annual mean basin-average ratios of the different hydrological fluxes to the total precipitation are represented as in Fig. 3. For each simulation, the first bar (top) corresponds to the runoff components: surface runoff (plain bar) and drainage (dashed bar). The second bar (bottom) corresponds to the evaporative fluxes, from the left to the right: bare soil evaporation (gray), plant transpiration (black), canopy interception loss (white), and ice (black) and snow sublimation (white). The ISBA-exp simulation is the control run with the same configuration as in section 4 ($d_c = d_2$ and $f = 2$ m^{-1}).

gauging stations against 30 for $f = 1$ m^{-1} and only 8 for $f = 3$ m^{-1}.

It should be also emphasized that the daily efficiency distributions of the simulation with a compacted depth of 1.5 m and the control run are very similar even if the NBSE criterion give a slight advantage to the control run. The daily efficiency distributions of the M simulation and of the control run also show comparable simulated discharge scores although the control run efficiencies are better at 59 against 29 gauging stations for the M simulation.

6. Discussion

The results of the high-resolution experiments show that the two versions of ISBA simulate well the annual discharge over the entire period. Nevertheless, Fig. 6 reveals that a deficiency of simulated runoff leads to a shortage in discharge during some rainy events. The Dunne mechanism alone, through the use of the TOPMODEL framework, does not seem to be able to account for this, and the lack of Horton runoff seems to be critical. Moreover, for hydrological applications, the

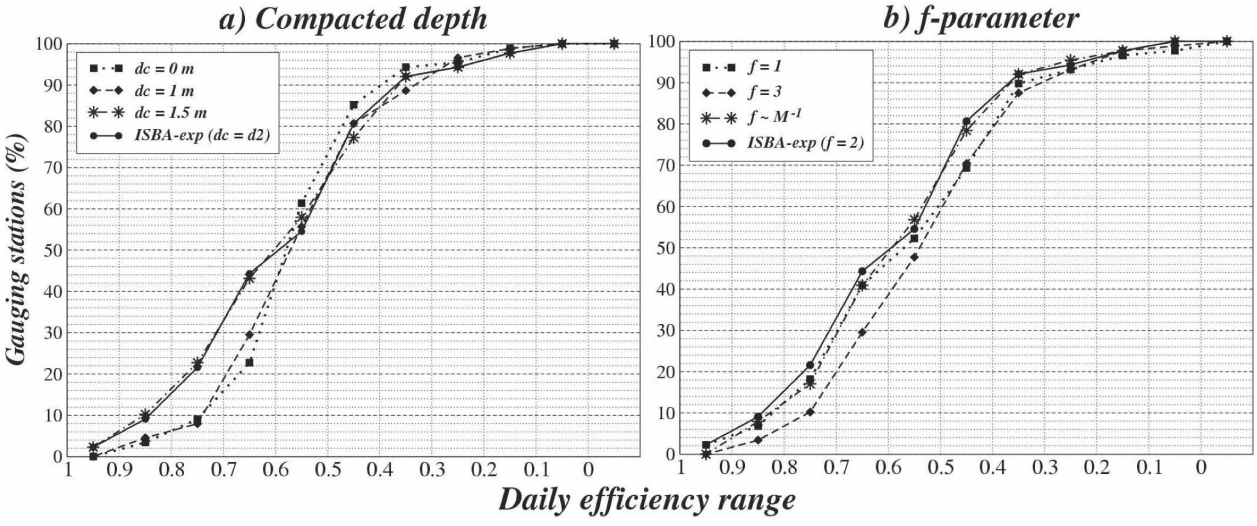

FIG. 11. Sensitivity to the compacted depth, d_c, and to the f parameter of daily river discharges simulated at the high resolution: (a) efficiency distributions with $d_c = 0$ m (plain squares), 1 m (plain diamond), and 1.5 m (stars) are shown, as well as (b) efficiency distributions with $f = 1$ m^{-1} (plain squares), 3 m^{-1} (plain diamond), and $\sim M^{-1}$ (stars). The control run is represented in each figure by plain circles. Statistics about these distributions are given in Table 6.

TABLE 6. Results of the sensitivity study experiments: statistics of the efficiency distribution of the simulated daily river discharges. Notations are the same as in Table 4.

Simulations	Min	Mean	Max	Std dev	NSBE
$d_c = 0.0$ m ($f = 2$ m^{-1})	0.09	0.53	0.86	0.14	37
$d_c = 1.0$ m ($f = 2$ m^{-1})	0.04	0.52	0.89	0.15	6
$d_c = 1.5$ m ($f = 2$ m^{-1})	0.08	0.55	0.90	0.19	45
Control run (ISBA-exp)	0.05	0.55	0.91	0.19	—
$f = 1$ m^{-1} ($d_c = d_2$)	−0.03	0.51	0.91	0.20	8
$f = 3$ m^{-1} ($d_c = d_2$)	−0.02	0.49	0.85	0.18	30
$f \sim M^{-1}$ ($d_c = d_2$)	0.06	0.54	0.89	0.18	50

fundamental land surface element is generally defined as the river catchment with boundaries defined by topography (Koster et al. 2000). Then, one can reasonably question whether the coupling strategy between ISBA and TOPMODEL, where the fundamental land surface element is a grid box (appendix A), is really suitable even if it is the most common strategy used by climate modelers (Chen and Kumar 2001; Warrach et al. 2002; Seuffert et al. 2002; Gedney and Cox 2003; Niu and Yang 2003). The watershed boundary-based formulation is certainly more physical but it implies a greater numerical cost. Moreover, the simulated discharges at high and low resolutions, as well as the relatively slight impact of aggregation on the simulated surface runoff, suggest that this simple approach is efficient. The main original assumption is that all TOPMODEL parameters only depend on soil properties, and that no calibration is needed. This is an important remark that justifies the use of the model for global-scale applications where calibration is difficult.

The simple parameterization of the exponential profile of k_{sat} introduced in ISBA can appear more questionable. Hydrological force–restore coefficients are usually calibrated with the help of multilayer scheme based on the Richards equations (Noilhan and Planton 1989; Boone et al. 1999). For the introduction of this new k_{sat} profile, this calibration appears difficult because, in addition to the textural properties, it the force–restore coefficients depend on a wide range of vertical grid configurations, and on a large number of combinations between the compacted depth and f. A more robust solution would be to replace the former homogeneous textural properties assumed in ISBA by a stratified soil (Montaldo and Albertson 2001). Nevertheless, the main constraint for climate modelers is that soil textural properties and their vertical profiles are poorly known at the global scale. Furthermore, the profile of k_{sat} is not only correlated with soil textural properties, but is also influenced by surface macrospores or large conducting channels created by organic matter, roots and/or agricultural human activity (Harr 1977; Beven 1984; Delire et al. 1997). The parameterization presented here has the advantage of simplicity and flexibility, while taking into account the essence of this physical phenomenon.

The exponential profile of k_{sat} has a clear impact on the simulated water budget and leads to different soil moisture equilibrium. When comparing ISBA-exp to ISBA, the fact that evapotranspiration is larger to the detriment of runoff is consistent with the results of Chen and Kumar (2001) over the entire North American continent. Nevertheless, the sensitivity experiments give some interesting insights. The simulation with a compacted depth, d_c, of 1.5 m is very similar to the control run ($d_c = d_2$) in terms of the water budget as well as quality of the simulated river discharges. This is because this simulation is performed with a compacted depth close to the basin-average rooting depth (1.54 m in Table 1). Therefore, the simulations assuming a decrease of k_{sat} directly from the surface ($d_c = 0$) or assuming a compacted depth of 1 m show poor discharge scores in comparison with the control run. These results confirm the relevance of an increase in k_{sat} from the uppermost few centimeters of soil to the rooting depth, in comparison with the values given by Clapp and Hornberger (1978). In addition, this conclusion points out that a compacted depth of 1 m as in Chen and Kumar (2001) is not sufficient to optimize the increase in k_{sat}. Boone et al. (2004) showed that simulating a reasonable ratio between surface runoff and total runoff is critical for producing realistic discharge over the Rhône River basin. The same conclusion was found by Lohmann et al. (1998) over the Red–Arkansas River basin. Results showing that the simulated discharge and the partitioning of total runoff into surface runoff and drainage is strongly sensitive to the choice of the compacted depth and to variations in f (Figs. 10 and 11) reinforce this conclusion and point out that the dynamics of the vertical water movements in the soil are also of primary importance. One general problem is that f, which is usually calibrated in small-scale hydrological applications, is extremely variable (Beven 1982b, 1997; Niu and Yang 2003). The M simulation, which gives acceptable results in terms of simulated daily river discharges, suggests that f could be simply related to soil properties [Eqs. (11) and (A6)]. This is an interesting result in the perspective of large-scale hydrological applications where calibration appears difficult and where there is no clear evidence that f should be spatially homogeneous.

The upscaling experiments show that the introduction of the exponential profile of k_{sat} does not perturb

the performance of ISBA in this kind of sensitivity experiment (Boone et al. 2004). On the contrary, the impact of spatial aggregation on total runoff and evapotranspiration is less sensitive with this new parameterization, and the improvement of the simulated discharges at the low resolution suggests that the new scheme is applicable at typical AGCM horizontal resolutions. However, further tests at the global scale are warranted in order to test if the assumption of an exponential profile of k_{sat} is acceptable, especially in arid areas where vegetation and organic matter are very sparse.

More generally, the scaling experiments show an overestimation in evapotranspiration and an underestimation in total runoff at the low resolution compared to the high resolution. The aggregation of vegetation and soil parameters, which tends to favor plant transpiration instead of total runoff, points out the need of subgrid variability in the land surface properties. As in Dolman and Blyth (1997), Boone et al. (2004), or Vérant et al. (2004), the dominant effect of the aggregated forcing, particularly of precipitation, is a strong increase in the canopy interception loss during the warm season. The lack of subgrid variability in precipitation and maximum infiltration capacity (Horton runoff) seems to be also critical, given the lack of simulated discharges during the rainy events (Fig. 6). The impact of upscaling the atmospheric forcing (not just precipitation) on runoff is also important, as it will be shown in a forthcoming study. The aggregation of the atmospheric temperature and longwave downwelling radiation leads to warmer conditions at the low resolution, which favors evapotranspiration instead of total runoff. In addition, snow mass and soil ice are underestimated, and sublimation is weaker than at the high resolution (Boone et al. 2004). Some models link subgrid topography (as altitude-dependent mosaic tiles) to some forcing variables, and show good scaling results because more snow falls in higher and colder tiles/regions at the expense of lower and warmer tiles/regions (Essery 2003; Boone et al. 2004).

7. Conclusions

This study presents the impact of an exponential profile of saturated hydraulic conductivity with soil depth on the water budget simulated over the French Rhône River basin, using the Météo-France ISBA LSM. The main hypothesis is that roots and organic matter favor the development of macropores and enhance the water movement near the soil surface, and that soil compaction is an obstacle for vertical water transfer in the deeper regions of the soils. This model version is compared to the original version in offline simulations using the same high- (8 km $\times$ 8 km) and low- ($1^\circ \times 1^\circ$) resolutions database as in the Rhône-AGG project (Boone et al. 2004).

These two comparisons show that the exponential profile of k_{sat} generally improves the simulated discharges. Therefore, it seems that an increase of k_{sat} from the soil surface to a depth close to the rooting depth, in comparison with values given by Clapp and Hornberger (1978), is a reasonable assumption. Nevertheless the partitioning of evapotranspiration is modified, since bare soil evaporation is favored to the detriment of plant transpiration. This results in a lower soil moisture equilibrium. Sensitivity studies of the parameters that control the exponential profile of k_{sat} show that their influence on the simulated water budget is relatively important. Very different river discharges are simulated, pointing out that the dynamics of the vertical water movements in the soil has a strong impact on discharge scores. In other words, soil vertical heterogeneities can be as significant as horizontal land surface heterogeneities. In addition, the improvement of the simulated river discharges at the low resolution suggests that this parameterization is also suitable for large-scale hydrological applications. This conclusion is reinforced by the fact that the exponential profile of k_{sat} reduces the impact of spatial aggregation on evapotranspiration and total runoff.

More generally, the high-resolution experiments point out that the Dunne mechanism, represented in this study through the use of the TOPMODEL formalism, is not sufficient to simulate daily discharges during heavy rain events, thereby emphasizing the need for a more comprehensive runoff scheme including the Horton runoff. The scaling experiment reveals that the low-resolution simulations with both model versions overestimate evapotranspiration. The largest impact is found with respect to the plant transpiration and canopy interception loss. In addition, the total runoff is notably underestimated. The lack of subgrid variability in precipitation and land surface properties, as well as in maximum infiltration capacity, seems to be critical. These results reinforce the general conclusions of several LSM intercomparison projects (Wood et al. 1998; Dirmeyer et al. 1999; Boone et al. 2004) that show that the main sources of subgrid variability are related to the spatial heterogeneities of precipitation, vegetation, soil properties, as well as topography, and that a parameterization of these subgrid phenomena at a low resolution, either through an explicit modeling of tiles or a statistical approach, is useful to properly partition precipitation between evapotranspiration and runoff.

Acknowledgments. The authors thank all their colleagues at the many French laboratories that have participated in the development of the Rhône modeling system (BRGM, CEMAGREF, CEPT, CIG, LTHE, Météo-France/CNRM, and CEN). We also wish to thank R. Koster and S. Mahanama for their availability and useful comments on the topographic-index computation. Finally, we gratefully acknowledge the assistance of N. Crouseilles (INRIA) for useful discussions related to the general mathematical framework. Thanks are also due to the anonymous reviewers for their constructive comments. This work was supported by Météo-France/CNRM and by the ACI "Observation de la Terre" of the French Research Ministry.

APPENDIX A

Surface Runoff Formulation

As in Habets and Saulnier (2001), the active layer used for the ISBA–TOPMODEL coupling is the rooting layer, and not the total soil column. TOPMODEL describes generally the evolution of a water storage deficit near the soil surface that reacts quasi-instantaneously following rainy events (Beven and Kirkby 1979). In that case, the root zone appears to be a reasonable compromise in ISBA.

More generally, the unit area A (m^2) is the traditional rectangular grid cell. For each pixel, i, of this area, a topographic index, $\lambda_i = \ln(a_i/\tan\beta_i)$ (m), where a_i (m) is the drainage area by unity of contour and $\tan\beta_i$ approximates the local hydraulic gradient, is defined. In other words, if the pixel has a large drainage area and a low local slope, its topographic index values will be large and, thus, its ability to be saturated will be high. In the derivation of the original TOPMODEL equations, the area mean deficit, D_t (m), is the integral of the local deficit, $d_{i,t}$ (m), over the catchments. With this assumption, the evolution of $d_{i,t}$ around its average value is thus linked to the difference between the local topographic index, λ_i, and its average value, $\bar{\lambda}$, by the relation $D_t - d_{i,t} = -M(\bar{\lambda} - \lambda_i)$; M (m) is a coefficient that describes the exponential decrease of soil transmissivity with local deficit: $T_{i,t} = T_0 \exp(-d_{i,t}/M)$ where T_0 is the surface transmissivity (Beven and Kirkby 1979; Beven 1997; Kirkby 1997). Therefore, for a given average deficit, the saturated pixels, for which $d_{i,t} \geq 0$, correspond to those where $\lambda_i \geq \lambda_{sat}$. The so-called saturated index, λ_{sat}, is the minimal value of the topographic index for which the basin is partially saturated. However, with this classical approach, the fraction of saturated area in comparison with the entire area is neglected. This approximation, for the area where the saturated part is important, can lead to a negative or to an underestimated mean deficit. Saulnier and Datin (2004) have suggested a corrected formulation, and an extension is made to the case where the local deficit is bounded in a defined range of values: $0 < d_{i,t} < d_0$, where d_0 is the maximum local deficit. Thus, the grid cell (or total basin) area, A, is divided in three subareas:

- A dry area, A_0, where the deficit is maximum: $d_{i,t} = d_0$ for all pixels where $\lambda_i \leq \lambda_0$.
- A wet area, A_{sat}, where there is no deficit: $d_{i,t} = 0$ for all pixels where $\lambda_i \geq \lambda_{sat}$.
- The area, $A - A_0 - A_{sat}$, where the deficit is $0 < d_{i,t} < d_0$ for all pixels where $\lambda_0 < \lambda_i < \lambda_{sat}$.

Here λ_0 is the dry index corresponding to the driest part, A_0, of the total area. Then, the new formulation for the area mean deficit is

$$D_t = \frac{1}{A}\left(\int_{A-A_0-A_{sat}} d_{i,t}\, dA + \int_{A_0} d_{i,t}\, dA + \int_{A_{sat}} d_{i,t}\, dA \right). \quad \text{(A1)}$$

Saulnier and Datin (2004) have shown that the next relation can link D_t to λ_{sat} as follows:

$$\frac{D_t}{M} = \frac{A - A_0 - A_{sat}}{A}(\lambda_{sat} - \bar{\lambda}') + \frac{A_0}{A}\frac{d_0}{M}, \quad \text{(A2)}$$

where $\bar{\lambda}'$ is the mean of the topographic index over the $(A - A_0 - A_{sat})$ area. The dry index, λ_0, is linked to λ_{sat} by

$$\lambda_{sat} = \lambda_0 + \frac{d_0}{M}. \quad \text{(A3)}$$

The maximum local deficit can be expressed as the difference between the saturation and the wilting point:

$$d_0 = (w_{sat} - w_{wilt}) \times d_2, \quad \text{(A4)}$$

and the relation between the grid cell average deficit and the soil moisture computed by the ISBA scheme can be simply expressed as

$$0 \leq D_t = (w_{sat} - w_2) \times d_2 \leq d_0. \quad \text{(A5)}$$

Then, it is possible to propose two new functions, $F(\lambda_{sat}) = D_t/M$ and $G(\lambda_{sat}) = A_{sat}/A$. The calculation of these functions is given in appendix B. A given average soil moisture, $w_2(t)$, is then associated with a mean deficit, D_t, and it is therefore possible to determine the saturated fraction, $f_{sat} = A_{sat}/A$, of the grid cell. In this case, the surface runoff is simply given by $Q_s = P_g \times f_{sat}$ where Pg ($m\,s^{-1}$) is the throughfall rate.

Because of the exponential decrease with deficit of the TOPMODEL transmissivity profile, the maximum

local deficit, $d_0 = 4 \times M$, represents more than 98% of the total transmissivity of the soil profile (Saulnier and Datin 2004). Then, the parameter M can be defined by

$$M = \frac{d_0}{4} = (w_{\text{sat}} - w_{\text{wilt}})\frac{d_2}{4}. \quad \text{(A6)}$$

For an average soil moisture, $w_2(t)$, lower than the wilting point, Eqs. (A4) and (A5) show that when the mean deficit is a maximum, $D_t = d_0$, $f_{\text{sat}} = 0$, and no surface runoff occurs.

Finally, the spatial distribution of the topographic index in each grid cell is computed with the three-parameter gamma distribution introduced by Sivapalan et al. (1987), and it is adjusted according to the linear regression of Wolock and McCabe (2000). The three parameters are derived from the mean, standard deviation, and skewness of the actual distribution given by the HYDRO1K dataset at a 1-km resolution (available online at http://edcdaac.usgs.gov/gtopo30/hydro).

Note that the TOPMODEL formalism is able to produce streamflow with both surface and subsurface runoff components. The subsurface runoff formalism given by TOPMODEL is not used here because it is very dependent on the inverse exponential values of λ_{sat} and on the value of k_{sat}. Therefore, errors on the topographic index calculation can lead to significant errors in the subsurface runoff calculation. Moreover, the subsurface runoff generated by TOPMODEL is negligible (Niu and Yang 2003) compared to the drainage produced by ISBA. It is less by two or three orders of magnitude due to the value of k_{sat} and to the inverse exponential values of λ_{sat}. For example, Chen and Kumar (2001) or Niu and Yang (2003) have introduced an anisotropic factor, accounting for the differences in k_{sat} in the lateral and vertical directions to simulate the desired streamflow response. In this case, k_{sat} in the lateral direction could be much higher by an order of two or three, and then, reasonable subsurface runoff is generated. Nevertheless, this factor is poorly known and must be calibrated basin by basin, which is a problem for large-scale hydrological applications.

APPENDIX B

ISBA–TOPMODEL Coupling: Algebraic Step

As already mentioned in appendix A, the spatial distribution of the topographic index in each grid cell is computed with the three-parameter gamma distribution introduced by Sivapalan et al. (1987):

$$\delta(\lambda_i) = \frac{1}{\chi\Gamma(\varphi)}\left(\frac{\lambda_i - \mu}{\chi}\right)^{\varphi-1} e^{[-(\lambda_i - \mu/\chi)]}, \quad \text{(B1)}$$

where the three parameters are derived from the mean, standard deviation, and skewness of the actual distribution (Sivapalan et al. 1987; Ducharne et al. 2000).

The relation (A2) can be revised as follows using $f_{\text{sat}} = A_{\text{sat}}/A$ and $f_0 = A_0/A$:

$$\frac{D_t}{M} = F(\lambda_{\text{sat}}) = (1 - f_{\text{sat}} - f_0)(\lambda_{\text{sat}} - \overline{\lambda}') + f_0\frac{d_0}{M}. \quad \text{(B2)}$$

Then, for each $\lambda_{\text{sat}t}$ [and λ_0 following Eq. (A3)], a mean deficit (D_t) over the grid cell can also be defined. The problem is to determine f_{sat}, f_0, and $\overline{\lambda}'$, which all depend on λ_{sat}.

Here $G(\lambda_{\text{sat}})$ and then f_{sat}, can be known simply by integrating $\delta(\lambda_i)$ from each λ_{sat} to the maximum value, λ_{max}, of the actual distribution [normalized to the entire integral of $\delta(\lambda_i)$ from the minimum value, λ_{min}, to λ_{max}, assuming numerical conservation]. In the same manner, f_0 is calculated by integrating $\delta(\lambda_i)$ from λ_{min} to λ_0. These integrals are calculated with the help of the so-called generalized incomplete gamma function given by Gautschi (1979) (http://www.netlib.org/toms/542).

Calculation of $\overline{\lambda}'$ is more problematic. It is defined as follows:

$$\overline{\lambda}' = \int_{\lambda_0}^{\lambda_{\text{sat}}} \lambda_i\delta(\lambda_i)\text{d}\lambda_i \Big/ \int_{\lambda_0}^{\lambda_{\text{sat}}} \delta(\lambda_i)\text{d}\lambda_i = I_1/I_2. \quad \text{(B3)}$$

As before, the integral I_2 is solved as for $G(\lambda_{\text{sat}})$ or f_0. The integral I_1 is solved after several algebraic steps. The result gives, assuming $y_i = (\lambda_i - \eta)/\chi$,

$$\overline{\lambda}' = \eta + \chi\left[\varphi + \frac{1}{\Gamma(\varphi)}\frac{y_0^{\varphi}e^{-y_0} - y_{\text{sat}}^{\varphi}e^{-y_{\text{sat}}}}{(1 - f_{\text{sat}} - f_0)}\right]. \quad \text{(B4)}$$

Finally, each TOPMODEL active layer volumetric water content can be estimated by defining another function, $W(D_t)$ [with the help of relation (A5)] as follows:

$$W(D_t) = w_{\text{sat}} - \frac{D_t}{d_2} = w_{\text{sat}} - \frac{MF(\lambda_{\text{sat}})}{d_2}. \quad \text{(B5)}$$

Then, the volumetric water content of the root zone, $w_2(t)$, is compared to $W(D_t)$ at each time step, and thus the instantaneous f_{sat} can be derived with the help of $G(\lambda_{\text{sat}})$.

REFERENCES

Ambroise, B., K. Beven, and J. Freer, 1996: Toward a generalization of the TOPMODEL concept: Topographic indices of hydrological similarity. *Water Resour. Res.,* **32,** 2135–2145.

Bélair, S., L.-F. Crevier, J. Mailhot, B. Bilodeau, and Y. Delage, 2003: Operational implementation of the ISBA land surface

scheme in the Canadian Regional Weather Forecast Model. Part I: Warm season results. *J. Hydrometeor.,* **4,** 352–370.

Beven, K. J., 1982a: Macropores and water flow in soils. *Water Resour. Res.,* **18,** 1311–1325.

——, 1982b: On subsurface stormflow: An analysis of response times. *Hydrol. Sci. J.,* **27,** 505–521.

——, 1984: Infiltration into a class of vertically non-uniform soils. *Hydrol. Sci. J.,* **29,** 425–434.

——, 1997: TOPMODEL: A critique. *Hydrol. Processes,* **11,** 1069–1085.

——, and M. J. Kirkby, 1979: A physically based, variable contributing area model of basin hydrology. *Hydrol. Sci. Bull.,* **24,** 43–69.

Boone, A., and P. Etchevers, 2001: An intercomparison of three snow schemes of varying complexity coupled to the same land surface model: Local-scale evaluation at an alpine site. *J. Hydrometeor.,* **2,** 374–394.

——, J.-C. Calvet, and J. Noilhan, 1999: Inclusion of a third soil layer in a land surface scheme using the force–restore method. *J. Appl. Meteor.,* **38,** 1611–1630.

——, V. Masson, T. Meyers, and J. Noilhan, 2000: The influence of the inclusion of soil freezing on simulations by a soil–vegetation–atmosphere transfer scheme. *J. Appl. Meteor.,* **39,** 1544–1569.

——, and Coauthors, 2004: The Rhône-aggregation land surface scheme intercomparison project: An overview. *J. Climate,* **17,** 187–208.

Braud, I., J. Noilhan, P. Bessemoulin, P. Mascart, R. Haverkamp, and M. Vauclin, 1993: Bare ground surface heat and water exchanges under dry conditions: Observation and parameterization. *Bound.-Layer Meteor.,* **66,** 173–200.

Brooks, R. H., and A. T. Corey, 1966: Properties of porous media affecting fluid flow. *J. Irrig. Drain. Amer. Soc. Civil Eng.,* **17,** 187–208.

Calvet, J.-C., and Coauthors, 1999: MUREX: A land-surface field experiment to study the annual cycle of the energy and water budgets. *Ann. Geophys.,* **17,** 838–854.

Champeaux, J. L., D. Acros, E. Bazile, D. Giard, J. P. Gourtorbe, F. Habets, J. Noilhan, and J. L. Roujean, 2000: AVHRR-derived vegetation mapping over western Europe for use in numerical weather prediction models. *Int. J. Remote Sens.,* **21,** 1183–1199.

Chapelon, N., H. Douville, P. Kosuth, and T. Oki, 2002: Off-line simulation of the Amazon water balance: A sensitivity study with implications for GSWP. *Climate Dyn.,* **19,** 141–154.

Chen, J., and P. Kumar, 2001: Topographic influence on the seasonal and interannual variation of water and energy balance of basin in North America. *J. Climate,* **14,** 1989–2014.

Clapp, R., and G. Hornberger, 1978: Empirical equations for some soil hydraulic properties. *Water Resour. Res.,* **14,** 601–604.

Deardorff, J. W., 1977: A parameterization of ground-surface moisture content for use in atmospheric prediction models. *J. Appl. Meteor.,* **16,** 1182–1185.

——, 1978: Efficient prediction of ground surface temperature and moisture with inclusion of a layer of vegetation. *J. Geophys. Res.,* **83,** 1889–1903.

Delire, C., J.-C. Calvet, J. Noilhan, I. Wright, A. Manzi, and C. Nobre, 1997: Physical properties of Amazonian soils: A modeling study using the Anglo-Brazilian Amazonian Climate Observation Study data. *J. Geophys. Res.,* **102,** 30 119–30 133.

Dirmeyer, P. A., A. J. Dolman, and N. Sato, 1999: The Global Soil Wetness Project: A pilot project for global land surface modeling and validation. *Bull. Amer. Meteor. Soc.,* **80,** 851–878.

Dolman, A. J., and E. M. Blyth, 1997: Patch scale aggregation of heterogeneous land surface cover for mesoscale meteorological models. *J. Hydrol.,* **190,** 252–268.

Douville, H., J.-F. Royer, and J.-F. Mahfouf, 1995: A new snow parameterization for the Météo-France climate model. Part I: Validation in stand-alone experiments. *Climate Dyn.,* **12,** 21–35.

Duan, J., and N. L. Miller, 1997: A generalized power function for the subsurface transmissivity profile in the TOPMODEL. *Water Resour. Res.,* **33,** 2559–2562.

Ducharne, A., D. R. Koster, M. J. Suarez, M. Stieglitz, and P. Kumar, 2000: A catchement-based approach to modeling land surface process in a general circulation model: 2. Parameter estimation and model demonstration. *J. Geophys. Res.,* **105,** 823–838.

Dümenil, L., and E. Todini, 1992: A rainfall–runoff scheme for use in the Hamburg climate model. *Adv. Theor. Hydrol.,* **9,** 129–157.

Durand, Y., E. Brun, L. Méridol, G. Guyomarc'h, B. Lesaffre, and E. Martin, 1993: A meteorological estimation of relevant parameters for snow schemes used with atmospheric models. *Ann. Glaciol.,* **18,** 65–71.

Essery, R. L., 2003: Aggregated and distributed modeling of snow cover for a high-latitude basin. *Global Planet. Change,* **38,** 115–120.

Etchevers, P., C. Colaz, and F. Habets, 2001: Simulation of the water budget and the rivers flows of the Rhône basin from 1981 to 1994. *J. Hydrol.,* **244,** 60–85.

Famiglietti, J. S., and E. F. Wood, 1994: Multiscale modeling of spatially variable water and energy balance processes. *Water Resour. Res.,* **30,** 3061–3078.

Gaiser, R. N., 1952: Root channels and roots in forest soils. *Soil Sci. Soc. Amer. Proc.,* **16,** 62–65.

Gautschi, W., 1979: A computational procedure for incomplete GAMMA functions. *ACM Trans. Math. Software*, **5,** 482–489.

Gedney, N., and P. M. Cox, 2003: The sensitivity of global climate model simulations to the representation of soil moisture heterogeneity. *J. Hydrometeor.,* **4,** 1265–1275.

Giordani, H., J. Noilhan, P. Lacarrère, and P. Bessemoulin, 1996: Modeling the surface processes and the atmospheric boundary layer for semi-arid conditions. *Agric. For. Meteor.,* **80,** 263–287.

Giordano, A., Ed., 1992: CORINE soil erosion risk and important land resources of the European community. EUR Tech. Rep. 13233 EN, 97 pp.

Habets, F., and G. M. Saulnier, 2001: Subgrid runoff parameterization. *Phys. Chem. Earth,* **26,** 455–459.

——, and Coauthors, 1999a: The ISBA surface scheme in a macroscale hydrological model applied to the HAPEX-MOBILHY area. Part I: Model and database. *J. Hydrol.,* **217,** 75–96.

——, P. Etchevers, C. Golaz, E. Leblois, E. Ledoux, E. Martin, J. Noilhan, and C. Ottlé, 1999b: Simulation of the water budget and the river flows of the Rhône basin. *J. Geophys. Res.,* **104,** 145–172.

——, P. LeMoigne, and J. Noilhan, 2004: On the utility of operational precipitation forecasts to served as input for streamflow forecasting. *J. Hydrol.,* **293,** 270–288.

Harr, R. D., 1977: Water flows in soil and subsoil on a steep forested slope. *J. Hydrol.,* **33,** 37–58.

Iorgulescu, I., and A. Musy, 1997: Generalization of TOP-

MODEL for a power law transmissivity profile. *Hydrol. Processes,* **11,** 1353–1355.

King, D., C. Lebas, M. Jamagne, R. Hardy, and J. Draoussin, 1995: Base de données géographiques des sols de France à l'échelle 1/1000000 (Geographical Soil Database for France at a scale of 1/1000000). Institut National de Recherches Agronomiques (INRA) Tech. Rep., Orleans, France, 100 pp.

Kirkby, M. J., 1997: TOPMODEL: A personal view. *Hydrol. Processes,* **11,** 1087–1097.

Koster, D. R., M. J. Suarez, A. Ducharne, M. Stieglitz, and P. Kumar, 2000: A catchement-based approach to modeling land surface process in a general circulation model: 1. Model structure. *J. Geophys. Res.,* **105,** 809–822.

Lohmann, D., and Coauthors, 1998: The Project for Intercomparison of Land-Surface Parameterization Schemes (PILPS) Phase-2c Red–Arkansas River Basin experiment: III. Spatial and temporal analysis of water fluxes. *Global Planet. Change,* **19,** 161–180.

Mahfouf, J.-F., and J. Noilhan, 1991: Comparative study of various formulations of evaporation from bare soil using in situ data. *J. Appl. Meteor.,* **30,** 351–362.

——, and ——, 1996: Inclusion of gravitational drainage in a land surface scheme based on the force–restore method. *J. Appl. Meteor.,* **35,** 987–992.

——, A. O. Manzi, J. Noilhan, H. Giordani, and M. Déqué, 1995: The land surface scheme ISBA within the Météo-France climate model ARPEGE. Part I: Implementation and preliminary results. *J. Climate,* **8,** 2039–2057.

Manabe, S., 1969: Climate and ocean circulation. I. The atmospheric circulation and the hydrology of the earth's surface. *Mon. Wea. Rev.,* **97,** 739–805.

Manzi, A. O., and S. Planton, 1994: Implementation of the ISBA parameterization scheme for land surface processes in a GCM: An annual cycle experiment. *J. Hydrol.,* **155,** 355–389.

Montaldo, N., and J. D. Albertson, 2001: On the use of the force–restore SVAT model formulation for stratified soils. *J. Hydrometeor.,* **2,** 571–578.

Nash, J. E., and J. V. Sutcliffe, 1970: River flow forecasting through conceptual models. 1, A discussion of principles. *J. Hydrol.,* **10,** 282–290.

Niu, G.-Y., and Z.-L. Yang, 2003: The versatile integrator of surface atmospheric processes (VISA). Part II: Evaluation of three topography-based runoff schemes. *Global Planet. Change,* **38,** 191–208.

Noilhan, J., and S. Planton, 1989: A simple parameterization of land surface processes for meteorological models. *Mon. Wea. Rev.,* **117,** 536–549.

——, and P. Lacarrère, 1995: GCM grid-scale evaporation from mesoscale modeling. *J. Climate,* **8,** 206–223.

——, and J.-F. Mahfouf, 1996: The ISBA land surface parametrization scheme. *Global Planet. Change,* **13,** 145–159.

Oki, T., T. Nishimura, and P. Dirmeyer, 1999: Assessment of annual runoff from land surface models using Total Runoff Integrating Pathways (TRIP). *J. Meteor. Soc. Japan,* **77,** 235–255.

Saulnier, G. M., and R. Datin, 2004: Analytical solving of a bias in the TOPMODEL framework water balance. *Hydrol. Processes,* **18,** 1195–1218.

Seuffert, G., P. Gross, C. Simmer, and E. F. Wood, 2002: The influence of hydrologic modeling on the predicted local weather: Two-way coupling of a mesoscale weather prediction model and a land surface hydrologic model. *J. Hydrometeor.,* **3,** 505–523.

Sivapalan, M., K. J. Beven, and E. F. Wood, 1987: On hydrologic similarity: 2. A scaled model of storm runoff production. *Water Resour. Res.,* **23,** 2266–2278.

Stieglitz, M., D. Rind, J. Famiglietti, and C. Rosenzweig, 1997: An efficient approach to modeling the topographic control of surface hydrology for regional and global climate modeling. *J. Climate,* **10,** 118–137.

Vérant, S., K. Laval, J. Polcher, and M. De Castro, 2004: Sensitivity of the continental hydrological cycle to the spatial resolution over the Iberian Peninsula. *J. Hydrometeor.,* **5,** 267–285.

Warrach, K., M. Stieglitz, H.-T. Mengelkamp, and E. Raschke, 2002: Advantages of topographically controlled runoff simulation in a soil–vegetation–atmosphere transfer model. *J. Hydrometeor.,* **3,** 131–148.

Wolock, D. M., and G. J. McCabe, 2000: Differences in topographic characteristics computed from 100- and 1000m resolution digital elevation model data. *Hydrol. Processes,* **14,** 987–1002.

Wood, E. F., and Coauthors, 1998: The Project for Intercomparison of Land-Surface Parameterization Schemes (PILPS) Phase-2c Red–Arkansas River Basin experiment: I. Experiment description and summary intercomparison. *Global Planet. Change,* **19,** 115–135.